



ISSN: 2454-9940



**INTERNATIONAL JOURNAL OF APPLIED
SCIENCE ENGINEERING AND MANAGEMENT**

E-Mail :
editor.ijasem@gmail.com
editor@ijasem.org

www.ijasem.org

Research on the Application of Frequency-Domain Correlation Method for RC Bridge Piers' Dynamic Response Evaluation and Impact Damage Identification

Perumallapalli Gandhi ¹, Dr G Raja Kumar ², Dr. B. Ravi ³

Assistant Professor ^{1,2,3}

Department of Mechanical engineering,

¹SV engineering college, Surya Peta (DIST). TS-508213

^{2,3}Swarna Bharati Institute of Science and Technology, Khammam, TS-507002

ABSTRACT:

We investigated the potential applications of damage correlation indices, which are correlation techniques based on the frequency domain, to enhance damage detection in reinforced concrete columns. Researchers used a new ultra-high drop hammer experiment method to hit four miniature reinforced concrete pier components, simulating the impact of medium-sized cars on bridge piers. The members' frequency response functions were assessed before and after the damage using an acceleration acquisition device. The experimental results demonstrated that the damage correlation indexes (DCI) taking into account the multi-order modal frequencies provided a reliable estimation of the pier damage levels. In addition, a modal analysis method and an impact finite element model were built and matched with the trials using the commercial program LS-DYNA. The collision processes between medium-sized cars and reinforced concrete piers were modelled by adjusting the finite element parameters in accordance with the experimental data. In order to guarantee that the structural design requirements are satisfied, a computation for the peak impact force (PIF) was provided for vehicle accident scenarios using damage indices.

Important terms: modal frequencies, damage detection, numerical models, reinforced concrete piers, and lateral impacts.

I.INTRODUCTION

Vehicles and transportation infrastructure in the area have expanded rapidly due to the steady quickening of urbanisation. The primary concern for the security of urban overpasses now is accidents involving bridge piers and cars. Numerous statistical studies on serious accidents caused by bridge collapses since the turn of the century have shown that incidents involving ships or vehicles striking bridges constitute around 20% of these events.¹ Particularly relevant in these instances are the uses of structural health detecting technologies. There may be obstacles to taking the required steps due to the large financial commitment required for damage assessments and restoration operations. Indeed, enhanced solution options for damage assessments have been made possible by advancements in sensor and computer technologies. New technologies, such as vibration-based monitoring systems, let engineers gather data in real-time, enabling real-time evaluation of structures by comparing original and damaged condition characteristics.² Data such as natural frequencies³, modal shapes⁴, mass values⁵, stiffness values⁶, damping matrices⁷, and frequency response functions (FRFs) are the most popular.⁸

There have been many countries that have proposed design codes to address the impact issues. The suggested AASHTO LRFD,⁹ is the most typical code; it designates bridge piers 1500 mm from the road edge with an equal static force of 2670 KN. The reasonability of the code was tested using the preliminary rough finite element model developed by Chen et al.¹⁰ The findings revealed that the values utilised in the

code were too cautious in some instances. The values given above were checked using the finite element model suggested by Abdelkarim and ElGawady¹¹. We compared these results with those from the similar static force calculation technique (equation (1)) offered by Euro-code and a 25 ms average peak force approach.¹² The findings suggested that the average force of the 25 ms peak force, as suggested by Buth et al.¹³, would be a more realistic static force equivalent for structural designs:

$$ESF = \frac{mv_r^2}{2(\delta_C + \delta_D)} \quad (1)$$

the vehicle's mass (m), its velocity (V_r), the distance (d_c) variable between the vehicle's head and its centre of mass, and the transverse deformation (d_D) of the column at the time of collision are all considered. A full-scale rigid pier model was subjected to transverse impact studies by Buth et al.¹⁴ using a 36t tractor-semitrailer. The model graphically displayed the mechanical behaviours of the bridge pier, such as the collision with the cargo pier and the crushing of the vehicle's head. Transverse impact studies were conducted using a medium-sized Dongfeng-EQ140 vehicle, and an anti-collision guardrail made of five short columns was designed by Chen et al.¹⁵. All sorts of data were captured during the testing procedures, including the impact force and deflection. A simpler finite element guardrail model was then proposed using the experimental data that had been gathered. Using a transverse impact experimental equipment, Cai et al.¹⁶ conducted impact tests on fifteen square scale columns. The previously stated research primarily focused on the impact energy, peak impact force, and member deformations as they relate to the slenderness ratios. Using an ultra-high drop-hammer experimental setup, Zhou et al.¹⁷ investigated the dynamic reactions of concrete pier components subjected to cumulative impact circumstances. A damage judgement technique based on variations in modal frequency was suggested, and the findings demonstrated that the buildings' internal energy dissipation capabilities had steadily declined as the damage degrees increased. Previous impact experiments

have undeniably contributed significantly to the advancement of numerical models in this domain. To reduce the weight of reinforced concrete beams, Adhikary et al.¹⁸ conducted experiments and developed a finite element model to examine several factors such as impact mass ratios, longitudinal reinforcement ratios, concrete compressive strength, and more. Furthermore, Pham and Hao¹⁹ verified the assumption of linear inertial force distributions along beams, developed a numerical model of reinforced concrete beams, and simplified the mechanical model to better capture the dynamic behaviours of these structures during impact processes. They also suggested a way to derive shear and bending moment diagrams. To replicate the forces exerted by heavy vehicles and reinforced concrete columns during impacts, Chen et al.²⁰ created a comparable impact frame. We then determined the equivalency values by comparing the deformations and internal energy relations of the frames with those of the real vehicles. The last step was to set up a suitable finite element simulation to confirm their general commonalities. Under several vehicle impact scenarios, Sharma et al.²¹ created finite element pier models and put up the idea of performance-based design to address impact issues. Furthermore, the damages were effectively identified under various conditions, and a suite of software frameworks was created to assess the capabilities and requirements of dynamic shear force in RC columns. Nevertheless, there is no practical and trustworthy quantitative metric, and the performance design criteria used to categorise bridge pier safety ratings are very imprecise. A computation approach for damage assessment indices and impact forces was developed in the research, which has great application. The piers in this investigation were subjected to simplified impact testing on a smaller scale utilising vehicles. The RC columns' dynamic reactions to impact were recorded, as were the modal frequency shifts after member damage. Next, a comprehensive finite element model was created based on the experimental data, and the findings were double-checked using the LS-DYNA software²². Along with it, we created a finite

element model of a full-scale pier subjected to impact. This study's numerical simulations showed the connections between the highest effect

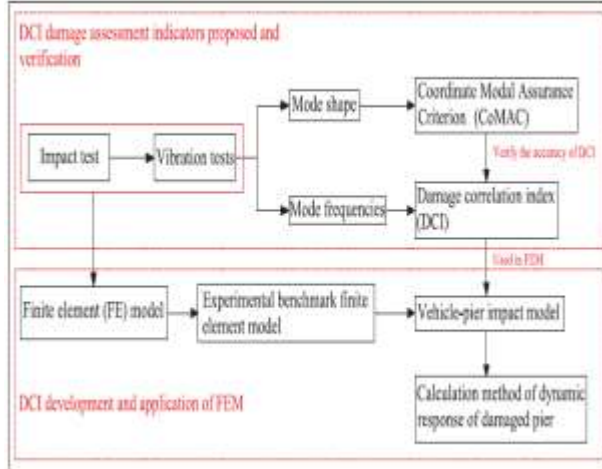


Figure 1. Technical route diagram of the experiments.

force (PIF) and the damage degrees. Then, an equivalent static force calculation formula of vehicle impacts in a short period of time was established with the damage of the bridge pier considered, which could potentially provide valuable references for future structural designs. The research methods involved in this article are shown in Figure 1.

Damage assessment methods based on frequency domains

An impact damage assessment approach that uses vibrations as its foundation is based on the fact that damage alters the dynamic response. Damage caused by a change in dynamic responsiveness may be detected by this occurrence. Here we provide two kinds of damage indicators. Specifically, there is the Coordinate Modal Assurance Criterion (CoMAC) and the Modal Assurance Criterion (MAC)^{23,24} This indication shows how the mode shape deviates before and after the reinforced concrete structure is damaged. One key distinction is that CoMAC takes into account deviations of the multi-order mode form, while MAC just takes into account deviations of the first-order mode shape. In the second place, we have the damage correlation coefficient (DCI), which may show how the multi-mode frequencies changed before and

after the damage to the structure. The target to be confirmed in this study is the damage index DCI suggested for impact damage, with CoMAC being regarded as a conventional damage assessment index.

2. MAC and Co MAC

The MAC is a dimensionless scalar constant, which represents the degree of correlation between the modal vector and another reference modal vector, as shown in equation (2). In the equation, CA_i represents the i -order modal vector from State A. The co-ordinate modal assurance criterion (CoMAC)²⁴ is an extension of the modal assurance criterion (MAC), and its correlation is modal related. As shown in equation (3), CA_{ij} is the j -order mode shape at point i in State A:

$$MAC(\{\psi_{A_i}\}, \{\psi_{B_j}\}) = \frac{|\{\psi_{A_i}\} \{\psi_{B_j}\}|^2}{(\{\psi_{A_i}\}^t \{\psi_{A_i}\})(\{\psi_{B_j}\}^t \{\psi_{B_j}\})} \quad (2)$$

$$COMAC(\{\psi_{A_{ij}}\}, \{\psi_{B_{ij}}\}) = \frac{\sum_{j=1}^N |\{\psi_{A_{ij}}\} \{\psi_{B_{ij}}\}|^2}{\sum_{j=1}^N \{\psi_{A_{ij}}\}^2 \sum_{j=1}^N \{\psi_{B_{ij}}\}^2} \quad (3)$$

Damage correlation index (DCI)

In this study, the damage degrees were evaluated by the differences or similarities between the original modal frequency and the damage modal frequency. The quantitative value was used to evaluate the differences between the two samples. The sample Pearson Correlation Coefficient (PCC)²⁵ in the form of a covariance was applicable to the problem. As shown in equation (4), A and B, respectively, represent the two states of health and damaged, A_i represents the i -th order modal frequency in the structural health state. \bar{A} is the mean value of the frequency sample in the healthy state, and σ_A is the standard deviation within the sample of this state:

$$PCC_{A,B} = \frac{\sum_{i=1}^n (A_i - \bar{A})(B_i - \bar{B})}{(n-1)\sigma_A\sigma_B} \quad (4)$$

$$\bar{A} = \frac{1}{n} \sum_{i=1}^n A_i \quad (5)$$

$$\sigma_A = \sqrt{\frac{1}{n-1} \sum_{i=1}^n (A_i - \bar{A})^2} \quad (6)$$

For real numbers with PCC value of [21,1], 1 represents the linear correlation; 0 represents the complete correlation; and 21 represents the reverse or indirect correlation between the data sets compared. However, such cases do not appear in this study since they represent the reverse correlation of the frequency. Therefore, assuming that PCC is bounded in the range of [0, 1], the damage correlation coefficient DCI could be calculated. It was not difficult to determine that the value of DCI was 0 when the column was undamaged and 1 when the correlation was completely lost:

$$DCI = 1 - |PCC_{A,B}| \in R \quad (7)$$

Experimental processes and analysis results

Two stages were used to achieve this goal: first, a lateral member percussive impact system; second, a member after damage vibration test, which assessed modal characteristics; and lastly, the influence of the effective loss characteristic index was studied. Four components of a 1:3 scaled bridge pier with a circular cross-section are built for this project. You may find the exact measurements of the bridge pier in the "Vehicle-bridge impact model" section, and the test model is scaled according to Buckingham's p theory. While pouring, check that the materials used for the full-scale bridge piers and the scaled components are same. The material properties' scaling impact is currently 1:1:

3. Experimental processes

Preparation of the damaged components. The detailed specimens are shown in Figure 2. Each specimen consisted of a 900 3 300 3 400 mm³ RC base and a circular RC column with a section radius of 170 mm and a height of 2200 mm. All of the specimens were cast using concrete with a cube compressive strength of 42 MPa.

The impact testing instrument was a super-high heavy-duty drop-hammer experimental testing machine system, which was composed of a vertical drop-hammer driving system and a horizontal impact system (Figure 3). As shown in Figure 3(a), the kinetic energy of the horizontal impact test vehicle was provided by the vertical drop-hammer driving system. The conversion relationship is shown in equation (8), where m1 and m2 represent the steel impactor mass and the drop weight mass, g is the

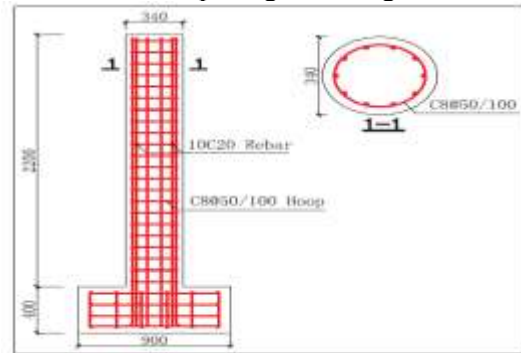


Figure 2. Specimen dimensions and detailed.

acceleration of gravity, h represents the release height of the drop weight, and m is the track dynamic friction coefficient. Table 1 details the basic information of the experimental components and the impacting scheme. The impact of the damage degree on the dynamic response of the column is reflected by the cumulative impact:

$$0.5 \times (m_1 + m_2)v_0^2 + \mu m_1 g = m_2 g h \quad (8)$$

Vibration tests. Following impact, the damaged components underwent modal testing for this investigation. Remove the axial load to rule out the possibility of axial force interference with the test, and keep the column's top half from vibrating. Figure 4(a) and (b) illustrate the vibration testing equipment. To make sure that the observed third-order modes were accurate, ten accelerometers were spread out in the direction of the hit specimen's back (Figure 4). Until the findings of the frequency measurements of the column are steady, the impact's front has been externally stimulated. It all started with the accelerometers taking readings of the pier's vibration properties during excitement; from there, the data was sent to the

data logger; finally, the computer gathered the last time domain signal and converted it to frequency domain data using Fast Fourier Transform. The damaged column C1 gathered acceleration time-domain data, which are shown in Figure 4(c). It is easy to see that the frequency of the damaged column diminishes with each rank, particularly at higher orders. The optimal quantity of accelerometers to guarantee precise experiment results.

Table 1. Information of the components

Specimen	Longitudinal reinforcement ratio ρ_L (%)	Hoop reinforcement ratio ρ_s (%)	Impact velocity at first record, steel loading (V_1 , T_1 , A_1) (m/s)	Axial compression ratio α_c (%)
C1	WCB (0.7)	MBB (1.7)	43	20
C2			45-45-45	20
C3		BB (0.8)	45-45	20
C4		BB (0.5)	45	20

The axial compression ratio is calculated by $\alpha_c = F_{ax} / (F_c + A_s f_y)$.

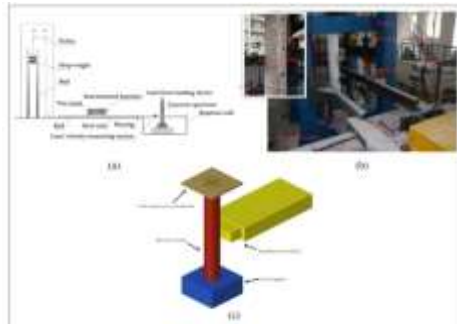


Figure 3. Impact testing system: (a) experimental set-up, (b) hardware impact system, and (c) FE model of the RC column with the steel impactor.

Evaluation of rigidity. This research will explain the stiffness variation using the total column stiffness as it is required to quantify the change in this parameter but it is not possible to discriminate shear and bending stiffness throughout the experiment. In order to remove the top rigid plate from contact with the column after impact, the axial pressure was released. At the very top of the column, the reaction wall delivered transverse forces of 100 kN, 200 kN, and 300 kN, in equal increments. Figure 5, where Dd stands for displacement differences, shows that a dynamometer was used to record the force magnitude, while a displacement meter mounted on the column's top was used to record the variations in displacement. The column stiffness was calculated using Equation (9), where E is the modulus of elasticity and I is the sectional moment of inertia.

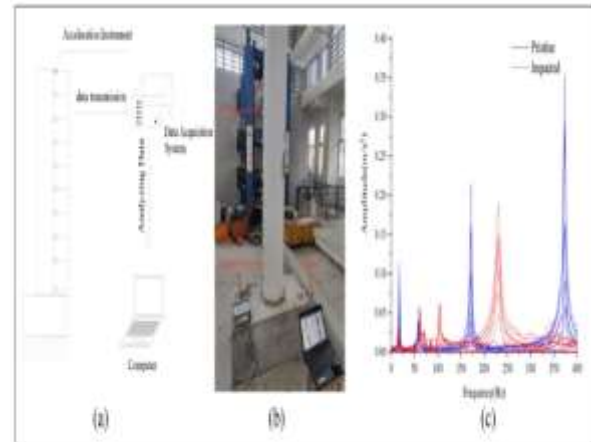


Figure 4. Modal testing system: (a) analytic flowchart, (b) experimental facility, and (c) comparison of frequency response plots of post-impact and original RC piers.

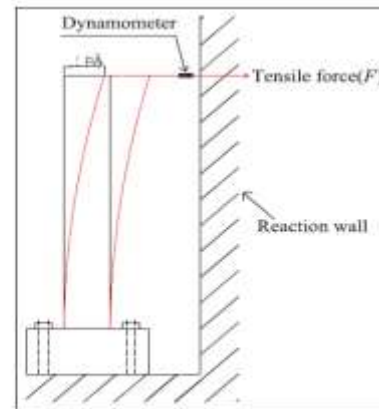


Figure 5. Stiffness measurement system.

$$K = \frac{3EI}{l^3} = \Delta F / \Delta \delta \quad (9)$$

4. Experimental results and analysis

Modal experiments. Experimental identifications of natural frequencies are included in this study's comparison in Figure 6 and Table 2. The results showed that the cracked areas had less stiffness as a consequence of the accumulated impacts. There was no regular pattern to the way the natural frequencies dropped as fractures formed.²⁶ At low damage levels, the change in first-order frequency was insensitive, making it impossible to characterize the damage level. Taking into account multi-order modal frequencies, the DCI computations revealed that this index was very vulnerable to harm. In contrast to the tendency of CoMAC's

development, the DCI will rise with increasing injury severity. It makes more sense to employ DCI as an assessment indication rather than only the first-order modal frequency.

The shifts in the modal forms were also impossible to ignore. The findings of the modal shape measurement of Component C2 before and after impact are shown in Table 3. Regardless of the variations in damage degrees, the first-order mode form remained the same. It was possible to make an initial determination as to where the damage was located, however, by watching how the second-order and third-order mode forms changed. The method's efficacy is shown by the dense fractures at this area.

Impact experiments. Figure 7 shows the relationships between the time history changes and the damage degrees of the three impact forces of component C2. As the degree of column damage increases, the column DCI increases and the peak impact force (PIF) decreases. The smaller losses in the stiffness values were found to have little effect on the peak impact force. However, the pier responses were noticeably weakened after two impacts. The lack of column stiffness resulted in the weakening of the responses.

Stiffness verification. The changes in the values of the stiffness of the components before and after impact were obtained using the method described in Section "Stiffness measurement." Table 4 details the statistics of the change rates of the stiffness values of all the components.

The decreases in the overall structural stiffness caused by the impacts resulted in changes in a series of natural frequencies. The development of this problem

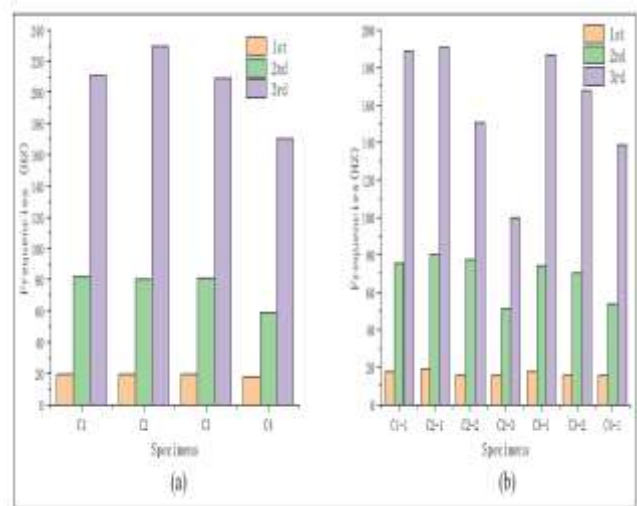


Figure 6. Modal frequencies of the components: (a) modal frequencies (undamaged) and (b) modal frequencies (damaged).

Table 2. Modal test results

Specimens	Experimental		FEM		CFMAC	DCI	
	Frequencies	DIFF (%)	Stiffness change (%)	FEM/PRSD			
C1	Undamaged			0		0	
	1st-order	19.53		18.98	3.82	1	
	2nd-order	82.02		80.46	3.63		
	3rd-order	316.99		205.44	3.54	0.931	
	Impact-1						
	1	17.87	-8.99	18.42	17.13	2.96	
	2	79.70	-7.71	79.81	73.81	4.24	
	3	188.75	-16.81	180.94			
	C2	Undamaged			0		0
		1	19.53		18.98	3.82	1
2		80.24		80.46	16.48		
3		328.49		205.44	16.22	0.984	
Impact-1							
1		18.08	-2.29	18.07	17.13	7.87	
2		79.79	-8.34	73.51	3.13		
3		190.73	-16.89	180.94			
C3		Undamaged			0		0
		1	19.53		18.98	3.82	1
	2	77.71	-2.15	73.53	4.66		
	3	153.26	-34.48	140.33	14.68	0.931	
	Impact-2						
	1	13.79	-19.76	15.73	3.88		
	2	77.71	-2.15	73.53	4.66		
	3	153.26	-34.48	140.33	14.68	0.931	
	C4	Undamaged			0		0
		1	19.21		18.98	3.89	1
2		81.21	-2.15	80.46	4.74		
3		308.73		194.67	3.18	0.877	
Impact-1							
1		17.38	-8.46	17.21	0.76		
2		74.30	-8.35	73.59	4.64		
3		186.31	-10.72	177.67	3.88	0.963	
C4		Undamaged			0		0
		1	17.87		17.98	3.29	1
	2	58.59		76.47	13.32		
	3	140.99		187.53	3.66	0.971	
	Impact-1						
	1	15.48	-11.91	13.98	14.73		
	2	53.34	-8.61	61.43	13.85		
	3	138.67	-18.43	133.71	3.82		

Table 2. (Continued)

Specimens	Experimental		FEM		CFMAC	DCI
	Frequencies	DIFF (%)	Stiffness change (%)	FEM/PRSD		
C4	Undamaged			0		0
	1	17.87		17.98	3.29	1
	2	58.59		76.47	13.32	
	3	140.99		187.53	3.66	0.971
	Impact-1					
	1	15.48	-11.91	13.98	14.73	
	2	53.34	-8.61	61.43	13.85	
	3	138.67	-18.43	133.71	3.82	

The DIFF under the Experimental describes the DIFF frequency of the column and the frequency change after column damage; the DIFF in the FEM describes the difference between the finite element calculation results and the experimental results.

Table 3. Comparison of the modal shapes of component C2.

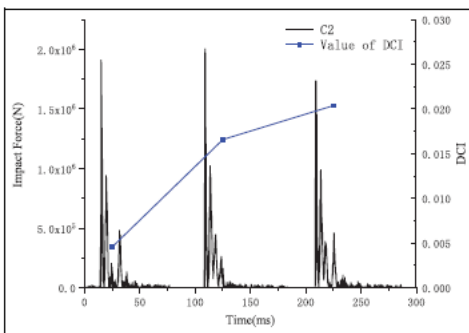
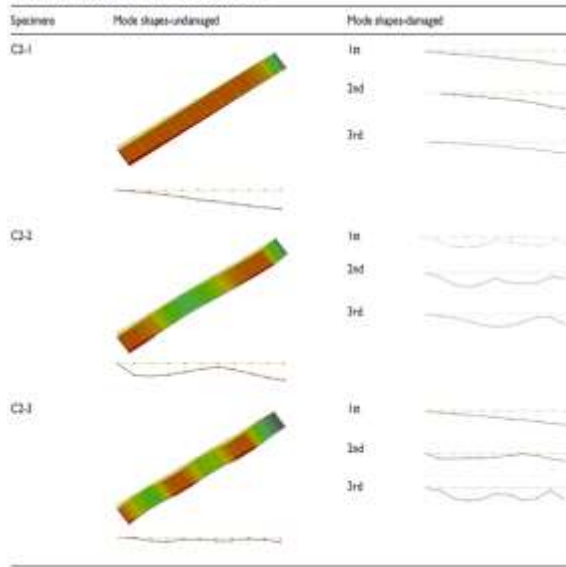


Figure 7. Comparison of the impact force time history and DCI changes of Component C2.

Table 4. Changes in the stiffness.

Specimen	Stiffness K (kn/m)	Change ratio (%)
C1		
Undamaged	8052.3	
C1-1	3976.4	50.62
C2		
Undamaged	7436.2	
C2-1	3734.8	49.77
C2-2	2357.7	68.29
C2-3	1529.6	79.43
C3		
Undamaged	6555.8	
C3-1	4192.8	36.04
C3-2	3479.6	46.92
C4		
Undamaged	6713.3	
C4-1	1444.6	78.48

mainly originated from the characteristic value problem of the system vibration equation. Therefore, motion equation (10) of the undamped mechanical system was applied. The first third order frequency approximation of the experimental model was solved using the Rayleigh Method²⁷ and the accuracy of the

experimental data was successfully verified. Therefore, in accordance with the principle of energy conservation, in which the strain energy at the maximum displacement time is equal to the initial kinetic energy, equation (11) was established.

$$\frac{\partial^2}{\partial x^2} \left[EI(x) \frac{\partial^2 v(x, t)}{\partial x^2} \right] + m(x) \frac{\partial^2 v(x, t)}{\partial t^2} = p(x, t) \quad (10)$$

$$U_{\max} = W_{\max} \quad (11)$$

The strain energy expression of a cantilever beam considering only the displacement in one direction is as follows:

$$W_{\max} = \frac{1}{2} \int_0^l EI \left(\frac{\partial^2 y}{\partial x^2} \right)^2 dx \quad (12)$$

The kinetic energy expression is as follows:

$$U_{\max} = \frac{1}{2} \omega^2 \int_0^l my^2(x) dx \quad (13)$$

Therefore, according to equations (10)–(13), the following was obtained:

$$\omega^2 = \frac{\int_0^l EI \left(\frac{\partial^2 y}{\partial x^2} \right)^2 dx}{\int_0^l my^2(x) dx} \quad (14)$$

In the current study, based on the above-mentioned method, the natural vibration frequencies of the cantilever components under the effects of gravity were solved and the first three order approximate solutions were determined as follows:

$$\omega_1 = \frac{3.5160}{l^2} \sqrt{\frac{EI}{m}} \quad \omega_2 = \frac{22.0345}{l^2} \sqrt{\frac{EI}{m}} \quad \omega_3 = \frac{61.6972}{l^2} \sqrt{\frac{EI}{m}} \quad (15)$$

The expressions of the structural stiffness were determined (equation (16)), and the structural stiffness were C3 obtained using the calculations detailed in Table 4:

$$K = \frac{3EI}{l^3} \Rightarrow EI = \frac{Kl^3}{3} \quad (16)$$

In this study, we confirmed the reliability of the experiments by comparing them to the outcomes of the theoretical calculations. It was clear from the results of the trials that the low-order frequencies were unaffected by the stiffness degradation phenomenon. The results of the measurements did not match up with the theoretical approximations because of this. Elastic treatments of the borders will be necessary to get more precise calculations as the

experimental techniques used in this work did not guarantee stable fixed boundaries. Still, as shown in Figure 8, the experimental data demonstrated good correlations between the DCI and changes in stiffness. Consequently, it was thought that in engineering, the recorded changes in component frequencies may be used to precisely forecast the degrees of stiffness loss.

Table 5. Comparison of the theoretical calculations and the experimental data.

Specimens	Frequencies (Hz)								
	1 st			2 nd			3 rd		
	Theo	Exp	Error (%)	Theo	Exp	Error (%)	Theo	Exp	Error (%)
C1	13.30	19.531	31.903	83.38	82.031	-1.645	232.46	210.993	-10.648
C1-1	9.35	17.578	46.809	58.59	75.703	22.685	164.06	188.953	13.174
C2	12.79	19.531	34.514	80.12	80.242	0.152	224.35	229.492	2.241
C2-1	9.06	19.083	52.523	56.78	79.791	28.889	159.00	190.736	16.639
C2-2	7.20	15.749	54.283	45.12	77.717	41.943	126.33	150.165	15.984
C2-3	5.80	15.749	63.172	26.34	50.781	28.488	101.75	99.609	-2.149
C3	12.00	19.213	37.542	75.23	81.212	7.366	218.65	288.73	-9.920
C3-1	9.60	17.588	45.417	60.16	74.304	19.035	168.47	186.214	9.577
C3-2	8.75	15.625	44.000	54.81	78.313	22.949	153.47	167.476	8.363
C4	12.15	17.578	30.880	76.13	58.994	-29.928	213.17	169.992	-25.400
C4-1	5.64	15.484	63.575	35.32	53.547	34.039	98.89	138.672	28.688

In the table, C1-1 represents the experimental data of the C1 member following the first impact. Test represents the experimental result.

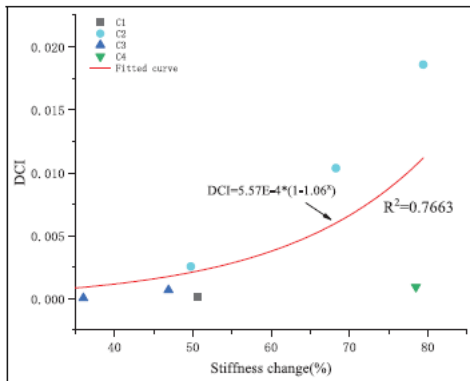


Figure 8. Correlations between the DCI and stiffness losses.

Numerical simulation and discussion

A finite element model which matched with the experiments was established using LS-DYNA commercial software. After analysis of the collision by explicit analysis, modal analysis by its implicit analysis. This section calibrates the finite element model and describes the solution to the conversion between algorithms.

Finite element (FE) model

The experimental model served as the basis for the 3D nonlinear finite element analysis model that was chosen, as seen in Figure 3(c). The impacting vehicles made of steel and concrete used hexahedral elements with one integral point, while the reinforcements were 2 3 2 Gauss

integral elements from Hughes-Liu sectional beams. A piecewise nonlinear model was also a reasonable way to characterise the longitudinal reinforcements and the stirrups, which were considered elastic-plastic materials. The strain rate effects were taken into account in this investigation using the dynamic intensification factor (DIF) relationships presented by Li and Hao28. Using equation (17), we were able to determine the correlations between strain rates and DIF. A multi-stage elastic-plastic curve was used to characterise the model. The material state description under quasi-static circumstances was $DIF = 1$ in the current experiment. When the stress level reaches 350 MP and the strain reaches 0.2%, the material shifts from an elastic to a plastic condition, which corresponds to the yield point. The experimental superstructure, an axial hydraulic loading platform, was represented in Figure 3(b). To apply the gravity load to the entire model, the numerical model made use of the keyword *LOAD BODY Z. The model was similarly simplified with an elastic material of appropriate mass. You might change the thickness of the elastic material to change its mass. Like the steel trolley, the RC construction was treated as an elastic material for calculations as its stiffness was much lower than the steel trolley's. You may find the material specifications in Table 6:

$$DIF_s = \left(\frac{\dot{\epsilon}}{10^{-4}} \right)^{0.074 - 0.040 \frac{f_c}{f_{t4}}} \quad (17)$$

In the current study, LS-DYNA contact keyword *CONTACT_SURFACE TO SURFACE contact algo- rithm was used between the mass object and column, and the keyword named *CONTROL_DYNAMIC_RELAXATION was used for the dynamic relaxation analysis of the structure 0.1 s prior to the calculation in

Table 6. Model material parameters.

Type	Material model	Parameter	Magnitude
Longitudinal rebar	PIECEWISE_LINEAR_PLASTICITY (**MAT_024)	Mass density	7850 kg/m ³
		Modulus of elasticity	205,000 MPa
		Poisson's ratio	0.3
		Yield stress	400 MPa
		Failure strain	0.4
Stirrup	PIECEWISE_LINEAR_PLASTICITY (**MAT_024)	Density	7850 kg/m ³
		Modulus of elasticity	205,000 MPa
		Poisson's ratio	0.3
		Yield stress	335 MPa
		Failure strain	0.4
Steel plates, Steel impactor	ELASTIC (**MAT_03)	Mass density	7850 kg/m ³
		Modulus of elasticity	205,000 MPa
Concrete	CSC Model (**MAT_159) ²²	Poisson's ratio	0.3
		Mass density	2490 kg/m ³
		Compressive strength	43 MPa
		Maximum aggregate size	15 mm
		EROD	1.1
		RECOV	10.4

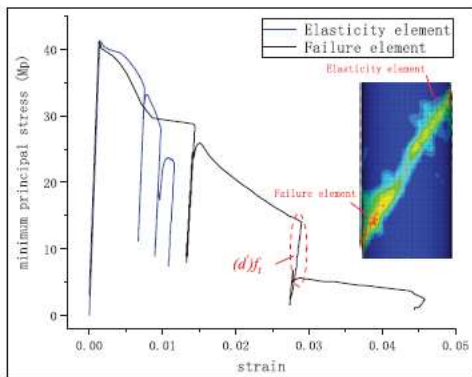


Figure 9. Cylinder model and result diagram.

order to ensure the stability of the axial force application. Then, based on the research results obtained by Yuan et al.²⁹ regarding grid size sensitivity, the concrete grid size was controlled at 10 mm. In addition, since the deformations of the steel impact trolley were very small during the contact processes, it could be regarded as a rigid body. Therefore, its grid was divided into 50 mm. In regard to the contact setting between the reinforcement and the concrete, CONstrain_BEAM IN SOLID was used to consider the slip effects between the reinforced concrete.

Concrete material model validation

The fact that the plastic deformation may be properly assessed and that unloading stress can occur reasonably is the key to proving that CSC is modal. In Figure 9, we can see Malvar's (model no. 30) basic finite element representation of the F150*300 mm cylinder. Cyclic loading was accomplished using displacement, and the cylinders' axial

compression trials were replicated. An earlier section detailed the material parameter settings. In Figure 9, we can observe the stress-strain development process of the elastic element and the failure element during loading. By comparing these data with experimental and finite element model results from literature, we can see that the model successfully captures the effects of stiffness degradation during damage accumulation processes. The concrete constitutive model also underwent trial calculations based on the experimental model. The experimental findings were compared with the numerical calculation results, and Figure 10 depicts the time history of the impact force and fracture formation of Component C4. In low-velocity impact scenarios, the findings demonstrated that the constitutive model could accurately forecast both the peak impact force and its evolution. Results from both the calculations and the experiments were found to be within a 10% margin of error.

Modal analysis of damaged model

Due to the oblique punching cracks (Figure 10) which occurred after impact, pre-existing damages were required in the numerical calculations. The pre-existing damage (PRED) parameters provided by the CSC model reasonably solved this issue. Modal analysis was

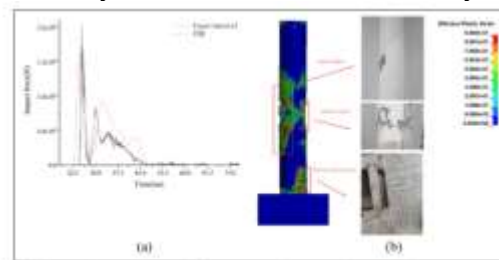


Figure 10. Experimental results of Component C4 and comparison of the value calculation results: (a) dynamic response of specimen C4 and (b) impact damage of specimen C4.

Table 7. Comparison of the modal frequencies under different damage degrees.

Modal frequencies/ PRED	0	0.1	0.3	0.5	0.7
1 st	22.0851	21.57	19.67	17.50	15.57
2 nd	98.4437	94.48	85.58	75.70	63.99
3 rd	238.4552	217.99	192.20	162.93	126.99

carried out for the same calculation model under different PRED values, and the results are shown in Table 7. It was found that the increases in the PRED values led to nonlinear reductions of the modal frequencies.

The use of restart technology opens the door to research into RC piers' cumulative damage issues and modal analysis. These issues were investigated experimentally and numerically by Kishi et al.³³. Nonlinear big deformation impact issues involving complex structures and many failure variables could not be solved using the KISHI approach, which was limited to problems involving collisions between simple rigid bodies. So, here is a new restart technique that this research provided: 1. After the first computation, the findings were double-checked with the help of the post-processing program Ls-Prepost, and the experimental data was compared. After validating the calculations, we used the export option in Ls-Prepost to export the element and node data. This allowed us to include these details into a geometric model for our next calculation.

2. Simultaneously, the DYNAIN option in Ls-Prepost was used to output the stress and plastic strain of all the elements upon completion of the first calculation. The material was initially damaged in order to create a stress-strain initialisation file at the start of the second calculation.

3. To acquire the second impact file, the solution settings, as well as the stress initialisation file and build a geometry file, were reset. By deleting the steel trolley and top steel plate and by setting the solver to implicit analysis, the model may be appropriately reduced during the construction of the modal analysis files.

In the current investigation, in order to ensure the accuracy of the modal calculations, the PRED values were adjusted in order to ensure that the MAC values

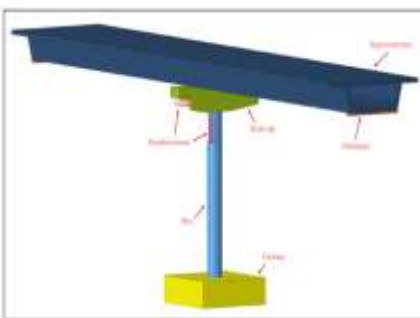


Figure 11. Specific sizes of the pier models.

were within a reasonable range. Then, the range was divided in order to facilitate the calculation process. Table 7 shows the numerical calculated modal frequency values. The results show that the calculation method is suitable for the present study.

Vehicle-bridge impact model

The DCI can also provide references for engineering designs. In order to study the relationships between dynamic responses and modal frequencies of bridge piers under the effects of cumulative impacts of vehicles, a large number of numerical simulation calculations were carried out using columns with different section sizes, and various impact velocities and vehicle masses. The results showed that there were two types of impact forces at the time of impact, which were controlled by the cargo mass and velocity values. It was found that according to the experimental results, the appropriate finite element analysis parameters could be determined. Then, when combined with the Ford F800 medium truck model developed by National Crash Analysis Center (NACA) and a full-scale model of the pier to verify the validity of DCI damage indicators used in this study. Through regression analysis, the relationship between damage degree and dynamic response was studied.

Information regarding the piers and vehicles

This research used the same material model, contact mode, and strain rate effect parameters as the one stated in Section "Concrete material model validation" to guarantee that the finite element model was valid. The dynamic response of a multi-span bridge may be efficiently predicted using a bridge model with two spans and two columns, according to Consolazio et al.; the prototype issue has been reduced to include a single column in a circular shape, a superstructure, and two supports. The concrete foundation, with dimensions of 5000 mm x 5000 mm x 1200 mm (as indicated in Figure 11), was to support a 30-meter-long superstructure by means of a trapezoidal solid beam mounted on top of the column. Its weight was adjusted in relation to the column section size to guarantee that the axial compression ratio remains constant in all collision circumstances. In Table 8, you

can see every single collision instance. A set of rubber bearings linked the column to the bridge pier's superstructure. Previous studies conducted by EI-TAWIL et al. shown that the total dynamic response of the pier is unaffected by the stiffness of the support. This section presupposes that the pier's vertical section will make contact with the concrete surface utilising the CONTACT AUTOMATIC SURFACE TO SURFACE keyword in LS-DYNA.

As shown in Figure 12, the Ford vehicle model was used to represent the collision of the vehicle on the bridge pier, Abdelkarim et al.11 and Sharma et al.21 shared the model and verified its accuracy through experimental tests. In this study's model, the total mass of the Ford truck was 8 t, including a 0.24 t engine mass and a 2.8 t cargo mass. The engine and cargo were simulated using elastic materials, with an elastic modulus of 11,000 MP and 2000 MP. The weight of the vehicle model was controlled by changing the quality of the goods.

Vehicle impact responses

Peak impact force (PIF). The change of damage degree is reflected by cumulative impact.. The typical time

Table 8. Numerical simulation of the component information.

Iteration	Column size (mm)	Longitudinal reinforcement ratio ρ_L (%)	Hoop reinforcement ratio ρ_s (%)	Axial compression ratio μ_a (%)
C800-V10-W8	800	18C22 (0.754)	25@150mm (0.31)	3881 (40.5)
C800-V96-W8				
C1000-V110-W8	1000	18C26 (0.784)	25@150mm (0.68)	4129.1 (40.5)
C1000-V96-W8				
C1200-V110-W8	1200	18C32 (0.711)	25@150mm (0.75)	8978.2 (40.5)
C1200-V96-W8				
C1200-V110-W8				
C1200-V96-W10				
C1200-V96-W12				
C1200-V110-W12				
C1200-V96-W12				
C1200-V110-W12				

In the table, C800-V96-W8-1 indicates that the 800mm diameter column is the first to be impacted by the vehicle with a total weight of 8 t and a speed of 40 km/h. *C22 means 40 steel bars with a diameter of 22mm. 25@150 means that the spacing is 150mm and the diameter is 25mm.

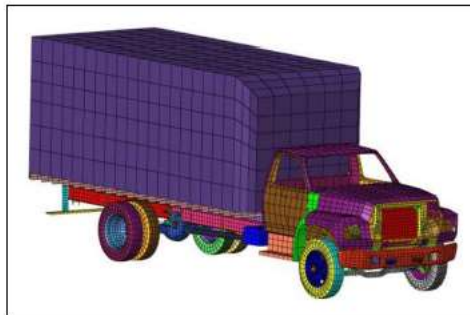


Figure 12. Truck model.

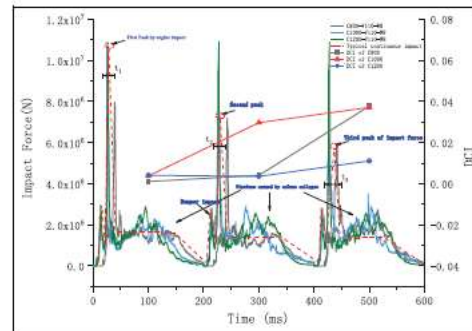


Figure 13. Time history diagram of the typical continuous impact force and damage degrees of the bridge piers.

history of the three consecutive impacts and corresponding DCI values are shown in Figure 13. A temporal graphical representation of the three impact forces (C800/1000/1200) acting on the V110-W8 part is shown in the figure. The second impact began at 400 ms and the third impact ended at 200 ms, with each calculation time being 200 ms. The engine's collision with the bridge pier was the common cause of the three impact forces' maximum values. Time history diagrams of the initial typical impact force and the impact force created by Chen et al.34 and Cao et al.35 were found to be compatible, according to the comparison findings. Figure 14 shows the component damage levels as a function of the effective plastic strain upon impact. The modal characteristics of the components deviated from their starting states as impact times accumulated, and PIF values decreased due to stiffness values decreasing. Researchers determined that this occurrence was typical of damaged piers. Also, it should be mentioned that this phenomena was not very noticeable in C1200-V110-W8. This was because the medium-sized truck's impacting effects at that speed were too weak to significantly alter the stiffness values of the pier of that specific size. Figures 13 and 14 display the data showing that the DCI values grow as the degree of damage does. Using DCI pier damage detection well will give you a better chance of surviving piers, whose value increases at a slower pace.

Table 9 details the statistical data of the numerical simulation results of the columns with different sizes, including the peak values, duration T_n , and 25 ms

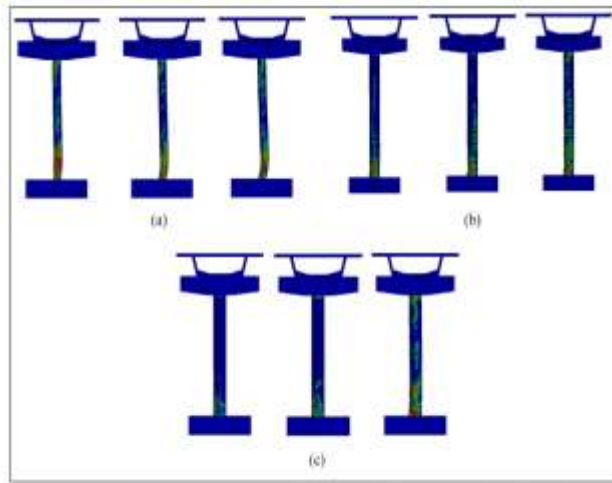


Figure 14. Comparison of the impact damage degrees: (a) C800-V110-W8, (b) C1000-V110-W8, and (c) C1200-V110-W8.

Table 9. Numerical simulation results.

Scenario	First impact			Second impact			Third impact		
	PF (MN)	SEF (MN)	DCI	PF	SEF	DCI	PF	SEF	DCI
C800-V10-W8	117	1.510	0.0013	1.51	1.946	0.0016	1.4	1.537	0.00736
C800-V90-W8	708	2.049	0.0060	4.31	2.121	0.01362	7.16	2.092	0.02769
C800-V110-W8	688	2.175	0.00405	7.86	2.526	0.01641	1.88	2.752	0.02779
C1000-V80-W8	112	1.450	0.0018	2.21	1.494	0.0018	2.15	1.530	0.00184
C1000-V90-W8	82	1.314	0.0019	4.72	2.327	0.00406	7.06	2.223	0.01655
C1000-V110-W8	88.9	1.423	0.00179	1.83	2.852	0.02911	6.38	2.718	0.05709
C1200-V80-W8	101	1.621	0.0019	3.23	1.634	0.01108	3.75	1.587	0.02445
C1200-V90-W8	848	2.224	0.0054	0.16	2.186	0.00453	4.4	2.176	0.00921
C1200-V110-W8	107	2.349	0.00411	0.07	2.333	0.00355	7.88	2.533	0.01107
C1200-V80-W10	107	1.681	0.0004	1.61	1.537	0.0011	2.70	1.554	0.00335
C1200-V90-W10	801	2.174	0.00515	4.88	2.150	0.00177	7.88	2.428	0.01308
C1200-V110-W10	11.9	2.325	0.00149	8.89	2.487	0.014437	8.39	2.408	0.02347
C1300-V80-W12	1.14	1.893	0.0023	1.57	1.949	0.002741	1.95	1.843	0.01451
C1300-V90-W12	814	2.353	0.00643	7.34	2.387	0.017594	4.17	2.181	0.02214
C1300-V110-W12	1228	2.333	0.00114	6.39	2.731	0.01881	6.32	2.642	0.02495

equivalent static calculation results of each impact force. All of the components in the table were impacted by a medium-sized vehicle of 8 t, which represented a typical type of engine impact scenario.

The studies conducted by EI-TAWIL [40] showed that the peak force formula (equation (18)) of ship-bridge impacts provided by American Association of State Highway and Transportation Officials (AASHTO) was also applicable to vehicle impacts. The impact velocity V (m/s) and the mass W (kg) of the impacting bodies were considered in the formula. In this study, a new expression equation (20) was proposed for the pre-damaged impact problem, and two dimensionless parameters, damage factor DCI, and the

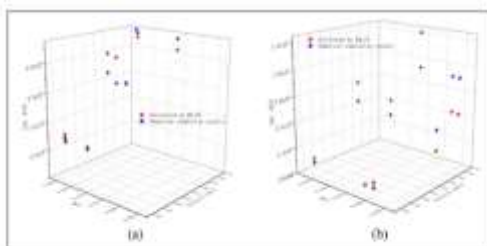


Figure 15. Comparison between simulation results and equation (20): (a) C1300-W10 and (b) C1300-W12.

equivalent stiffness ($b/800$) were introduced. Therefore, the formula was able to achieve a more comprehensive description of each parameter. Five regression coefficients (referred to as a , b , c , d , and e) were determined using a nonlinear regression analysis method. It was found that when subjected to continuous impacts, the PIF engine could be estimated using equation (20). Figure 15 details this study's comparison of the fitting results and the numerical simulation results

$$F_i = f\{\alpha(V)^{\beta}(W)^{\gamma}\} \quad (18)$$

$$PIF = f\left\{a(DCI)^b(V)^c(W)^d\left(\frac{b}{800}\right)^e\right\} \quad (19)$$

$$PIF_{engine} = 10027.08(DCI)^{-0.044}(V)^{2.13}(W)^{-0.085}\left(\frac{b}{800}\right)^{0.364} \quad (20)$$

5. Conclusion

The bridge piers hit by low-speed vehicles were examined for damage and their structural safety using the frequency domain-based correlation approach (DCI), which was introduced in this study. We confirmed its usefulness and feasibility. The study's results led to the following conclusions:

The fundamental procedures in the proposed strategy were the measurement of the frequency response functions of structures with impact damages and the application of fast Fourier transform (FRFs) processing to derive the modal frequency characteristics of the structures. The intrinsic frequencies of the columns were discovered to be significantly affected by the cracking processes. The impacts also reduced the columns' stiffness values at the fracture sections and caused nonmonotonic decreases in the modal frequencies. This means that structural damage correlation indexes (DCIs) may be calculated and compared using the collected data. Findings showed that DCI was capable of making accurate predictions about structural damage level and residual stiffness values.

2. The precision of the reference experimental model is confirmed, and methods for calculating modal identification after structural damage and impact on reinforced concrete columns based on the finite element approach are presented.

3. The pre-damaged vehicle-pier impact events

were computed using a finite element approach in the present research inquiry. The maximum impact force was predicted using the DCI and equation (20). The suggested formula outperformed the results of comparable studies because it accounted for the decreases in impact force and the loss of stiffness due to structural flaws. This meant that subsequent stages of structural design may benefit from the suggested approach.

References

1. Cook W, Barr PJ and Halling MW. Bridge failure rate. *J Perform Constr Facil* 2015; 29: 04014080.
2. Gomes GF, Mende'z YAD, Alexandrino PSL, et al. The use of intelligent computational tools for damage detection and identification with an emphasis on composites: a review. *Compos Struct* 2018; 196: 44–54.
3. Perez MA, Gil L and Oller S. Impact damage identification in composite laminates using vibration testing. *Compos Struct* 2014; 108: 267-276.
4. Zenzen R, Belaidi I, Khatir S, et al. A damage identification technique for beam-like and truss structures based on FRF and Bat algorithm. *CR Me'canique* 2018; 346: 1253–1266.
5. Liu S, Zhang L, Chen Z, et al. Mode-specific damage identification method for reinforced concrete beams: concept, theory and experiments. *Constr Build Mater* 2016; 124: 1090–1099.
6. Sha G, Cao M, Radzien'ski M, et al. Delamination-induced relative natural frequency change curve and its use for delamination localization in laminated composite beams. *Compos Struct* 2019; 230: 111501.
7. Sampaio RPC, Silva TAN, Maia NMM, et al. Damage identification based on response functions in time and frequency domains. In: Nobari AS and Ferri Aliabadi MH (eds) *Vibration-based techniques for damage detection and localization in engineering structures*. China: World Scientific Publishing Co Pte Ltd, 2018, pp. 197–236.
8. Pe'rez MA, Pernas-Sa'nchez J, Artero-Guerrero JA, et al. High-velocity ice impact damage quantification in composite laminates using a frequency domain-based correlation approach. *Mech Syst Signal Process* 2021; 147: 107124.
9. Officials AAoSHaT. *AASHTO-LRFD. Bridge design specifications – customary US Units*. 5th ed. Washington, DC: Officials AaoSHaT, 2010.
10. Chen L, El-Tawil S and Xiao Y. Reduced models for simulating collisions between trucks and bridge piers. *J Bridge Eng* 2016; 21: 04016020.
11. Abdelkarim OI and ElGawady MA. Performance of bridge piers under vehicle collision. *Eng Struct* 2017; 140:337–352.
12. Al-Thairy H and Wang YC. An assessment of the current Eurocode 1 design methods for building structure steel columns under vehicle impact. *J Constr Steel Res* 2013; 88: 164–171.
13. Buth CE, Brackin MS, Williams WF, et al. *Collision loads on bridge piers: phase 2, report of guidelines for designing bridge piers and abutments for vehicle collisions*. Bryan, TX: Texas Transportation Institute, 2011.
14. Buth CE, Williams WF, Brackin MS, et al. *Analysis of large truck collisions with bridge piers: phase 1, report of guidelines for designing bridge piers and abutments for vehicle*

- collisions. Bryan, TX: Texas Transportation Institute, 2010.
15. Chen L, Xiao Y, Xiao G, et al. Test and numerical simulation of truck collision with anti-ram bollards. *Int J Impact Eng* 2015; 75: 30–39.
16. Cai J, Ye JB, Chen QJ, et al. Dynamic behaviour of axially-loaded RC columns under horizontal impact loading. *Eng Struct* 2018; 168: 684–697.
17. Zhou XW, Zhou M, Gao YS, et al. An evaluation study on the cumulative impact damages of reinforced concrete piers based on modal frequencies. *Eng Fail Anal* 2021; 119: 104983.
18. Adhikary SD, Li B and Fujikake K. Dynamic behavior of reinforced concrete beams under varying rates of concentrated loading. *Int J Impact Eng* 2012; 47: 24–38.
19. Pham TM and Hao H. Influence of global stiffness and equivalent model on prediction of impact response of RC beams. *Int J Impact Eng* 2018; 113: 88–97.
20. Chen L, Wu H and Liu T. Shear performance evaluation of reinforced concrete piers subjected to vehicle collision. *J Struct Eng* 2020; 146: 04020026.
21. Sharma H, Hurlebaus S and Gardoni P. Performance-based response evaluation of reinforced concrete columns subject to vehicle impact. *Int J Impact Eng*. 2012; 43: 52–62.
22. Murray YD. Users manual for LS-DYNA concrete material model 159. No. FHWA-HRT-05-062. Washington, DC: United States Federal Highway Administration Office of Research, Development, and Technology, 2007.
23. Pastor M, Binda M and Harčarik T. Modal assurance criterion. *Procedia Eng* 2012; 48: 543–548.
24. Allemang RJ. The modal assurance criterion – twenty years of use and abuse. *Sound Vib* 2003; 37: 14–23.
25. Ahlgren P, Jarneving B and Rousseau R. Requirements for a cocitation similarity measure, with special reference to Pearson's correlation coefficient. *J Am Soc Inform Sci Technol* 2003; 54: 550–560.